Ionics
https://doi.org/10.1007/s11581-019-02916-7

ORIGINAL PAPER

Tailoring of the structural, morphological, electrochemical, and dielectric properties of solid polymer electrolyte

Anil Arya[1] · A. L. Sharma[1]

Received: 10 October 2018 / Revised: 30 January 2019 / Accepted: 6 February 2019

Abstract

A solid polymer electrolyte composed of poly(ethylene oxide) and sodium hexafluorophosphate has been synthesized with a varying fraction of succinonitrile via solution cast technique. Impedance spectroscopy, transference number measurements, and linear sweep voltammetry were used to study the electrochemical properties. The 10 wt.% succinonitrile system exhibited the highest ionic conductivity of $\sim 2 \times 10^{-5}$ S cm^{-1} which is two orders of magnitude higher than the pristine polymer salt system. The high ionic transference number (~ 1) confirms that ion conduction is dominated by ions and displays the voltage stability window of about 4 V. The dielectric permittivity and the relaxation time ($\tau_{\varepsilon'}$, τ_M, τ_h) values corresponding to the segmental motion of the polymer chain varies with the variation of succinonitrile content. The relaxation time and double-layer capacitance are in good agreement with the conductivity. Finally, an ion transport mechanism has been proposed to provide a better understanding of ion migration.

Keywords Solid polymer electrolyte · Amorphous content · Ionic conductivity · Relaxation time

Introduction

The lithium-ion batteries (LIB) are the most fascinating candidate for the portable electronics, electric vehicles since its commercialization in 1991 by SONY corporation. The LIB possess advantages such as high energy density, long cycle life but some drawback restricts its use, i.e., high cost, less abundant, and environmental impact. Sodium ion battery (SIB) is an excellent alternative to the LIB and conveys subsequent advantages over LIB; (i) Na is highly abundant, (ii) low cost, and (iii) suitable redox potential ($E^{o}_{Na^{+}+Na} = -2.71$ V versus standard hydrogen electrode; only 0.3 V above that of lithium) [1–4]. The development of polymer electrolyte (PEs) in order to substitute the traditional liquid electrolyte for energy storage devices (e.g., battery and supercapacitor) has attracted the widespread attention of scientific community due to advantages such as safety, flexibility, varied shape geometry, good interfacial and compatibility.

So, new materials were developed by incorporating low molecular weight plasticizers in the polymer salt matrix known as gel polymer electrolytes (GPEs). Although the GPEs have comparable ionic conductivity (10^{-3} S cm^{-1}) to the liquid electrolyte, the poor mechanical strength/safety and liquid plasticizer prevent their use as an electrolyte in the commercial applications. To overcome the above issues, a solvent-free system was, i.e., solid polymer electrolyte (SPE) was launched and has gained momentous research interest and has potential to replace liquid/gel polymer electrolyte which has drawbacks such as flammability, leakage issue, and bulky in size. One key advantage with SPE is that it plays a dual role, (i) works as a separator as well as electrolyte and (ii) acts as a binder to improve the interfacial contact with electrodes. However, SPE possesses lower ionic conductivity at ambient temperature. To overcome the poor ionic conductivity, various approaches are manifested to develop new materials such as polymer blending, nanofiller dispersion, and incorporation of ionic liquids/plasticizer [5–16].

Poly (ethylene oxide) is the most popular candidate among all polymers due to its interesting characteristics, low glass transition temperature (T_g), attached electron rich ether group (−O−) in polymer backbone (−CH_2 − CH_2 − O−), desirable dielectric constant ($\sim$4–5), and a broad range of salt complexation [17]. But the semi-crystalline nature of PEO results in

✉ A. L. Sharma
alsharma@cup.edu.in

[1] Department of Physical Sciences, Central University of Punjab, Bathinda, Punjab 151001, India

Published online: 21 February 2019

lower ionic conductivity. It is well-known that the amorphous phase supports fast ion transport in case of polymer electrolytes [18]. The sodium hexafluorophosphate ($NaPF_6$) was chosen as salt to provide ions due to advantages, (i) weak interaction between cation and anion, (ii) large anion size, and (iii) greater salt dissociation, hence reduce the chance of ion pair formation [19–21].

The incorporation of the plastic crystals in the polymer matrix is an interesting approach for conductivity enhancement which is interpreted by assuming the effective role of the plasticization effect. Succinonitrile (SN; N≡C–CH_2–CH_2–C≡N) is an interesting candidate as compared to the traditional plasticizer and is chosen due to high polarity, high dielectric constant (~ 55). The role of abovesaid characteristics property is interpreted in three ways, (i) the presence of polar nitrile group in SN will improve the salt dissociation and number of free charge carriers, (ii) SN penetration between polymer chain will provide more free volume for ion migration, and (iii) disruption of covalent bonding between polymer chains will promote the faster chain segmental motion. The simultaneous presence of the above properties will enable a favorable ion migration, and hence high ionic conductivity [22].

In our present study, free standing solid polymer electrolyte based on PEO as a host polymer, sodium hexafluorophosphate ($NaPF_6$) as salt, with different SN content are prepared by solution cast technique. The structural, morphological, microstructural, and electrochemical investigations are carried out. Then, the dielectric study covering the complex permittivity, complex conductivity, and the modulus formalism were explored in the frequency range 1 Hz-1 MHz. The dielectric plots were fitted to evaluate the dielectric strength, relaxation time, hopping time, and dc conductivity. Finally, we proposed an interesting interaction scheme to understand the role of constituents of solid polymer electrolytes in enhancing the ion transport.

Methodology

Materials

The polymer PEO (av. mol. wt. 600,000 g/mol), sodium hexafluorophosphate ($NaPF_6$), succinonitrile (SN), and anhydrous acetonitrile were purchased from Sigma Aldrich. The polymer and salt are dried under vacuum at 50 °C for 24 h before use.

Electrolyte preparation

PEO-$NaPF_6$ (O/Na = 8) + x wt.% SN polymer electrolytes were prepared by the standard solution cast technique. In this process, the appropriate amount of PEO and $NaPF_6$ were dissolved separately followed by stirring of combined solution until a homogenous and viscous solution is obtained. Then, varying content of SN was added in the polymer salt complex and stirred again till a viscous solution is obtained. The obtained solution is poured into Petri dishes and left at room temperature to evaporate the solvent. After solvent evaporation, the films were kept in a vacuum oven to completely remove the solvent. Finally, the thin dry film was peeled off and kept in a vacuum desiccator for further investigations. The samples were designated as PE-x where x = 1, 2, 3, 4, 5. PE 1 designates the pure PEO and PE 2 designates the polymer salt complex (PEO-$NaPF_6$); PE 3 to PE 5 is designated for the x wt.% of SN added (10, 15, 20%) in PEO-$NaPF_6$ sample. It may be noted that the further increase of SN content in polymer salt complex results in poor quality of the films, hence not investigated.

Characterization

The field emission scanning electron microscopy (FESEM) was used to investigate the surface morphology of prepared polymer electrolyte. The structural investigations were recorded by the X-ray diffraction (XRD) (Bruker D8 Advance) with Cu-K_α radiation having a wavelength (λ) 1.54 Å in the Braggs angle range (2θ) from 10 to 60°. The Fourier transform infrared (FTIR) spectra (Bruker Tensor 27) was performed in the wavenumber region 600–3500 cm^{-1} to confirm the various interactions between constituents of the polymer electrolyte. The ionic conductivity was measured by electrochemical impedance spectroscopy (EIS) using electrochemical analyzer (CHI 760; USA) over a frequency range of 1 Hz to 1 MHz and an AC signal of 10 mV is was applied to the cell configuration *SS|SPE|SS*. The ion transference number was measured by i-t characteristics by applying a dc voltage of 10 mV. The electrochemical voltage stability window was measured by linear sweep voltammetry technique (LSV) and cyclic voltammetry (CV) with cell configuration *SS|SPE|SS*. To investigate the dielectric properties, the impedance data was used to obtain the dielectric parameters such as complex permittivity and complex conductivity which are further transformed into the real and imaginary parts of the modulus.

Results and discussion

Field emission scanning electron microscope (FESEM) analysis

The FESEM micrographs of the pure PEO (Fig. 1a) display the rough morphology with some smoother surface due to semi-crystalline nature. Then, the addition of salt alters the surface morphology significantly which is noticeable clearly from Fig. 1b and is comparatively smoother than Fig. 1a. This may be due to complexation between the polymer host with

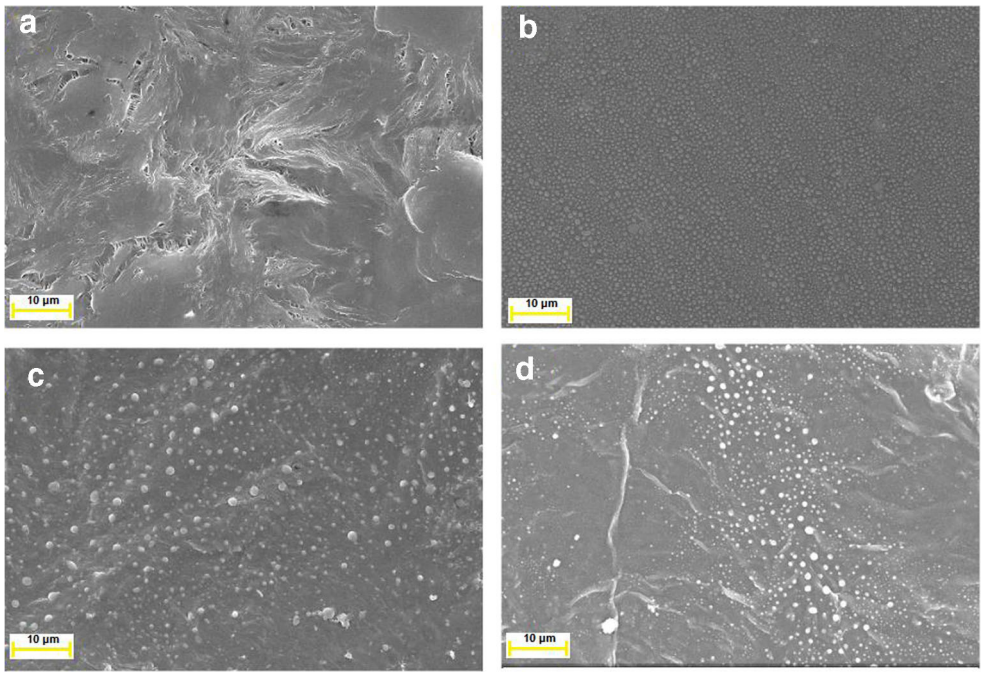

Fig. 1 FESEM surface morphology of **a** PEO, **b** PEO-$NaPF_6$, **c** PEO-$NaPF_6$-10% SN, and **d** PEO-$NaPF_6$-20% SN

the cation (Na^+) of salt. Addition of SN in the polymer salt matrix results in the smoother and homogenous surface (Fig. 1c). The smooth surface is associated with the ease of ion migration and will be analyzed in the forthcoming section. The addition of very high SN content results in the insulating effect of SN due to improper mixing as visible in Fig. 1d [23].

X-ray diffraction (XRD) analysis

To examine the effect of SN addition on the crystallinity, interchain separation, and inter-planer spacing, we performed the XRD analysis. Figure 2 shows the comparison of XRD diffractograms of the pure PEO, PEO-$NaPF_6$, and PEO-$NaPF_6$- containing x wt.% SN ($x = 10$, 15, 20). It may be noticed from the diffraction pattern of pure PEO, two peaks are located at 19.03° and 23.1° corresponding to the (120) and (112/032) reflection planes. These peaks are primarily due to the crystalline nature of PEO and agree with the literature [24]. Figure 2b shows the reduction in peak intensity of PEO peaks that confirm the disruption of polymer chain arrangement owing to the interaction between the polymer matrix and salt. It indicates the complex formation between the cation of salt and the ether group of the polymer host. This interaction enhances the amorphous content. Although, with the addition of salt, some additional peaks are observed, that are not of pure PEO and $NaPF_6$. These peaks are attributed to the presence of ion-multiplets (as Na_2X^+, NaX_2^-) [21, 25, 26]. Further, the absence of any $NaPF_6$ peak reveals the complete dissociation of salt and complex formation is confirmed [27–29]. After addition of SN in the polymer salt matrix, the lowering in the intensity of the PEO peak located at 19.03° and 23.1° evidences the effective role played by SN. The addition of SN having polar nitrile group in its structure promotes the salt dissociation and disruption of the crystalline arrangement of the PEO chains. The reduction of peak intensity clearly indicates that the addition of SN enhances the amorphous content and promotes the faster segmental motion, hence the increase of ionic conductivity in the polymer matrix [30].

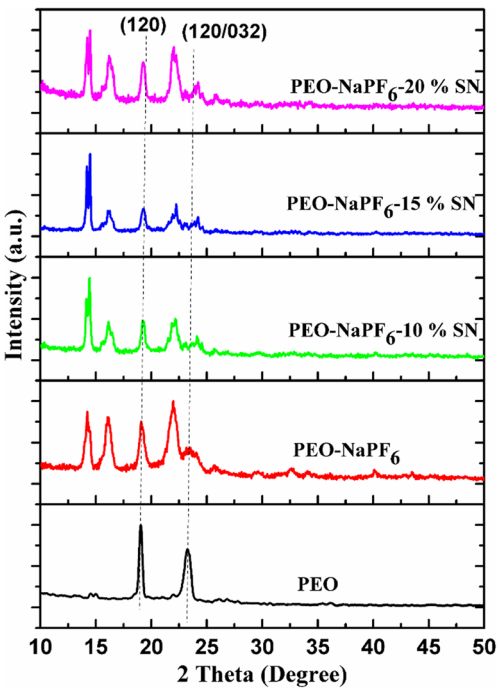

Fig. 2 XRD patterns of the PEO, PEO-$NaPF_6$, and PEO-$NaPF_6$- x wt.% SN ($x = 10$, 15, 20)

To support the above results, the d-spacing, crystallite size L of the PEO, and interchain separation were calculated using the $2d\sin\theta = n\lambda$, $L = 0.94\lambda/\beta\cos\theta$, and $R = 5\lambda/8\sin\theta$, respectively. The increase in the d and R value on the addition of plasticizer indicates the plasticizer penetration in between polymer chains. This weakens the covalent bonding between polymer chains and makes easier polymer chain motion that facilitates the cation migration. The reduction of the crystallite size corresponding to (120) reflection plane confirms the complex formation. The crystallinity values of all the prepared sample have been calculated using the formula; X_C $(\%) = (A_C/(A_C + A_A)) \times 100$, where A_C and A_A are the areas for the crystalline peaks of PEO and amorphous peak areas respectively. It has been calculated using the standard Origin8 software. The crystallinity value is summarized in Table 1 and it decreases with addition of SN [12]. This evidences that incorporation of SN affects the polymer Skelton, and reduction of crystallinity indicates the availability of favorable volume for faster ion migration. This was confirmed by the Table 1, which shows the increase in the interchain separation (R) for all polymer electrolyte with SN addition and comparatively large R is noticed than pure PEO and polymer salt complex.

Fourier transform infrared (FTIR) spectrum analysis

The interactions of salt and SN with the polymer host are investigated by the FTIR spectra. The FTIR absorbance spectra of the solid polymer electrolyte with salt and with x wt.% ($x = 0, 10, 15, 20$) SN are shown in Fig. 3 and band assignment is summarized in Table 2. It is found that the pure PEO spectrum shows the C–O stretching vibration mode at 956 cm^{-1}. The fundamental peak of the PEO is the C–O–C stretching mode located at 1106 cm^{-1}. The CH_2 symmetric twisting, CH_2 asymmetric twisting, CH_2 bending mode, and CH_2 wagging mode are observed at 1236 cm^{-1}, 1282 cm^{-1}, 1347 cm^{-1}, and 1465 cm^{-1} respectively [31]. It may be noted from the FTIR spectrum that all the groups of PEO, salt, and SN are present; it indicates the complex formation of PEO, $NaPF_6$, and SN. After the addition of the salt, the CH_2 twisting and CH_2 bending group show modification in the peak shape and shift in peak position. The band located at 1465 cm^{-1} is ascribed to CH_2 wagging mode and displays reduction of peak intensity with the addition of the salt. The peaks in the wavenumber region 2800 to 2950 cm^{-1} are ascribed to the symmetric and asymmetric vibration of C–H stretching mode of CH_2 group in PEO. The spectrum shows the change in peak intensity that evidences the polymer-salt interaction [32, 33]. Further addition of SN alters the peak shape as well as position and indicates the complexation between the constituents of solid polymer electrolytes. Although the characteristics peak still remains in the spectrum, some alterations are noticed. The peak of C–O–C stretching mode located at 1106 cm^{-1} is strongly affected after SN addition and get broadened with the addition of SN; also, peak intensity gets reduced. The obtained reduction in the peak intensity is attributed to the cation (Na^+) coordination with the lone pair of electrons (ether group) on PEO [34]. So, from the FTIR analysis, it can be concluded that the complexation of the salt and polymer occurs and the result is in absolute agreement with the XRD and FESEM results.

Table 1 Values of 2θ (°), d-spacing (Å), R (Å), and crystallite size L, and crystallinity of PEO-$NaPF_6$ with x wt.% SN (10, 15, 20)

Sample	(120) diffraction peak				Crystallinity (%)
	2θ (degree)	d-spacing (Å)	R (Å)	L (nm)	
PE 1	19.03	4.66	5.82	24.60	43
PE 2	18.87	4.69	5.87	11.94	43
PE 3	18.73	4.73	5.91	16.08	42
PE 4	18.58	4.76	5.94	16.40	38
PE 5	18.36	4.82	6.02	15.76	40

Impedance study

The ionic conductivity of the solid polymer electrolytes (SPE) has been investigated at room temperature by sandwiching the polymer electrolyte membrane in the cell configuration SS|SPE|SS. Figure 4 shows the impedance plot (Z'' vs. Z') in the log-log presentation. The advantage of log-log representation is summarized somewhere [21]. It may be noted that the impedance plot shows two arcs, (i) toward lower frequency and (ii) toward high frequency [35, 36]. The second arc at high-frequency side suggests the ion migration in the amorphous phase of the polymer matrix, and the first arc toward lower frequency side is associated to the double layer capacitance effect formed at the electrode-electrolyte interface [37–40]. With the addition of SN, the high-frequency arc disappears and indicates that total conductivity is owing to the cation only ($\sigma = ne\mu$). The same feature has been reported earlier also [41, 42]. Although, the nature of the plot is the same for all solid polymer electrolytes with some change in the arc shape. The solid red line is the fitted plot using software ($Z_{SimpWin}$). The experimental and fitted data are in good agreement with each other. The equivalent circuit is shown in the inset. It comprises of a resistance in series with the parallel combination of constant phase element (Q) and another resistance. The first resistance is the electrolyte resistance while the second resistance is associated with the transfer of ions at the electrode/electrolyte surface. The presence of constant phase element infers the presence of non-ideal capacitive behavior [43, 44].

The ionic conductivity (σ) of the prepared polymer electrolyte has been determined using the equation: $\sigma = L/(R_b \times S)$;

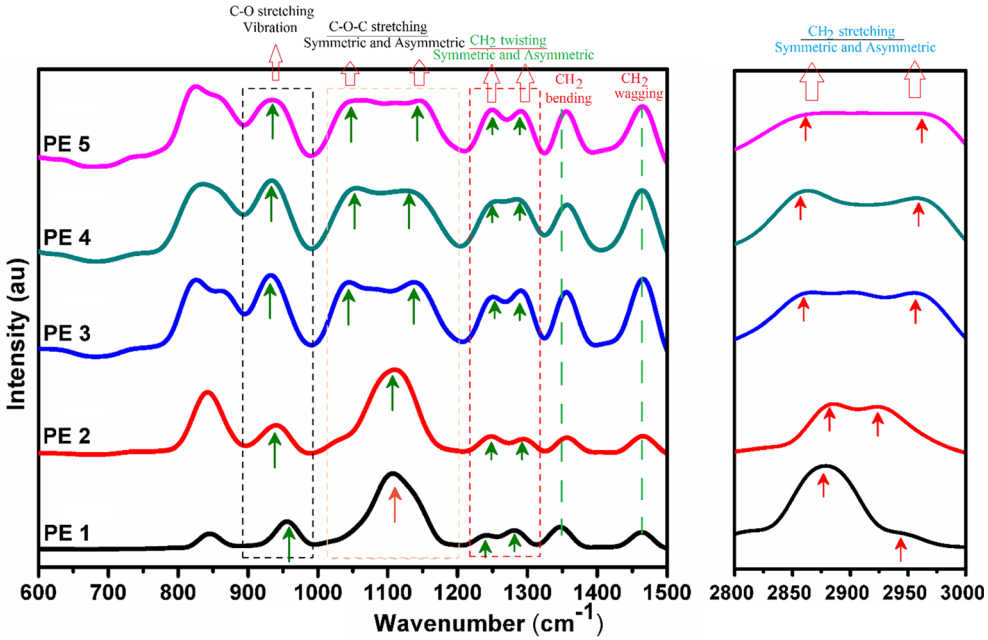

Fig. 3 FTIR spectra of pure PEO (PE 1), polymer salt (PE 2), and with *x* wt.% of SN (*x* = 10, 15, 20) (PE3-PE5)

were, L is the thickness of the polymer electrolyte (100–125 μm), S is the area of the blocking electrode (1.43 cm^2) and R_b is the bulk resistance of polymer electrolyte films. The dip observed in the impedance plot (corresponds to minima in Z'') gives an estimate value of the bulk resistance, and addition of salt in pure PEO shows decrease of bulk resistance. As bulk resistance is inversely proportional to conductivity value, so a decrease in the bulk resistance indicates the increase in the conductivity of prepared SPE. Therefore, the enhancement in the ionic conductivity is due to the following reasons, (i) availability of more number of ion charge carriers due to better salt dissociation after SN addition, (ii) faster ion mobility, and (iii) increase in the free volume and amorphous phase for the ion migration. It may be concluded from the above results that the addition of SN in the polymer salt complex promotes the migration of the cation via polymer chain segmental motion. While, at higher SN-content decrease in conductivity is evidenced that may be associated with the increased crystalline arrangement (dense structure). This prevents the easier ion migration due to disruption of continuous path owing to small amorphous phase, and overall negative consequence on conductivity is witnessed. Another reason may be the loss of contact with electrodes owing to the sample stiffness [45, 46]. The above analysis suggests the correlation between the structure of electrolyte and electric properties. This is also in agreement with the XRD results that show the decrease of crystallinity evidenced by reduction of intensity.

The polymer electrolyte system PE4 is an optimized sample and exhibits the highest conductivity 1.92×10^{-5} S cm^{-1}, which is three orders higher than the pure polymer, two orders higher than the polymer salt complex. Another important parameter is, double layer capacitance that is calculated using the formula, $C_{dl} = -\frac{1}{\omega Z''}$; w here ω is the angular frequency and Z'' is the imaginary part of impedance at low frequency. It is interesting to note that the SPE system with the highest value of the ionic conductivity possesses the highest double layer capacitance (C_{dl}). The increase in the conductivity is further investigated in terms of dielectric properties in the forthcoming section.

Transference number

In the case of solid polymer electrolytes, both ions and electrons are active species. So, to completely understand the enhancement of the ionic conductivity, it is important to separate out the ionic and electronic contribution [47, 48]. Ionic transference number was measured by Wagner's DC polarization technique at a fixed applied voltage (20 mV) across the cell SS/SPE polymer electrolyte/SS (@ RT). The variation of polarization current is plotted against the time for the polymer salt complex (PE 2), and SN-incorporated polymer electrolytes (PE 3, PE 4, PE 5::10, 15, 20 wt.% SN) at room temperature are shown in Fig. 5. For all systems, the initial current decreases with time followed by a steady with the passage of time. The initial current is the contribution of both the ions and the electrons ($I_t = I_e + I_i$) while the later one is the contribution of electrons only because of blockage of ions at the electrode-electrolyte interface [49–51]. The obtained ion transference number is 0.99 (close to unity). This infers that the total conductivity is mainly due to the flow of ions and electron contribution to total conductivity is negligible, which is desirable for the solid state ionic conductor (Table 3). Also, the transference number close to unity eliminates the issue of concentration polarization during cell operation [52].

Table 2 FTIR spectral data of PEO, PEO-$NaPF_6$, and SN-added PEO-$NaPF_6$-based solid polymer electrolyte

Wavenumber (cm^{-1})					Band assignment
PE 1	PE 2	PE 3	PE 4	PE 5	
845	842	827	831	824	C–O stretching in PEO and PF_6^- vibration
956	938	933	933	935	C–O stretching vibration
1106	1107	1044/1139	1050/1134	1047/1143	Symmetric and asymmetric C–O–C stretching
1236	1246	1251	1251	1249	CH_2 symmetric twisting
1282	1294	1291	1287	1292	Asymmetric CH_2 twisting
1347	1356	1354	1354	1354	CH_2 bending
1465	1465	1467	1464	1464	CH_2 wagging
2877	2882	2864	2858	2858	Symmetric C–H stretching
2948	2922	2956	2960	2962	Asymmetric C–H stretching

The ionic and electronic conductivity are also calculated through suitable equations, $i_t = i_i + i_e$, $\sigma_{ionic} = \sigma_{electrical} \times i_i$, $\sigma_{electronic} = \sigma_{electrical} \times i_e$. The high value of ionic conductivity and negligible electronic conductivity evidence that the charge transport in the investigated system is due to ions only.

Electrochemical stability window

The electrochemical voltage stability window or working voltage range of SPE has been measured by linear sweep voltammetry (LSV) and cyclic voltammetry (CV) technique which is sandwiched in cell assembly SS (blocking electrodes)/SPE polymer electrolyte/SS (blocking electrodes) at RT (scan rate 10 mV/s) [53]. The LSV and the CV curves are shown in Fig. 6 and Fig. 7, respectively. Figure 6 shows the steady current up to 3 V and after that rapid increase in the current flows which is due to the electrolyte decomposition [54]. The voltage stability window of the SPE containing SN displays improved stability (3.5–3.9 V) as compared to polymer salt system (3.3 V). It suggests that there is no decomposition of the electrolyte at least up to this range (~4 V). The enhancement in the voltage stability window suggests the use of SPE in the high voltage practical applications within a safe limit.

The enhancement in the electrochemical stability window (ESW) is further supported by the cyclic voltammogram (Fig. 7). The ESW is the region where no faradic current flows and is evaluated by the cathodic/anodic component where the oxidation/reduction of solid polymer electrolytes is observed [55]. The absence of any oxidation-reduction peak in CV confirms the better electrochemical stability of the prepared solid polymer electrolyte. The solid polymer electrolyte with highest ionic conductivity shows ESW in the range −2 and 2.1 V. This gives ESW of about 4.1 V. It may be noted that after SN addition, broadening in ESW is evidenced and all solid polymer electrolyte shows ESW of about ~4 V. From the results, it may be concluded that the prepared SPE possesses desirable voltage stability window for the practical applications.

Dielectric analysis

Real (ε') and imaginary (ε'') part of complex permittivity (ε^*)

The complex permittivity (ε^*) investigations of solid polymer electrolyte are crucial to understanding the polarization effect at the electrode-electrolyte interface [56–58]. The frequency dependent complex dielectric permittivity comprises of two parts, real part (ε') designates polymer electrolyte polarizing ability that indicates charge storage capacity or storage capacity of a material on application of field. The imaginary part, i.e., dielectric loss (ε'') is a measure of the energy required to align the dipoles. The complex permittivity (ε^*) is expressed as $\varepsilon^* = \varepsilon' - j\varepsilon''$.The real and imaginary part of complex permittivity are used to simulate the experimental data [58, 59].

The complex dielectric permittivity is expressed by Eq. 1:

$$\varepsilon^* = \varepsilon' - j\varepsilon''; \varepsilon' = \frac{-Z''}{\omega C_o\left(Z'^2 + Z''^2\right)} \text{ and } \varepsilon'' = \frac{Z'}{\omega C_o\left(Z'^2 + Z''^2\right)} \quad (1)$$

Where, where ε' and ε'' are the real and imaginary parts of the dielectric permittivity respectively. The real and imaginary parts of dielectric constant can obtained by separating above equation and can be given as Eq. 2 a and b [55, 57, 58].

$$\begin{cases} \varepsilon' = \epsilon_\infty + \dfrac{\Delta\varepsilon\left(1 + x^\alpha \cos\dfrac{\alpha\pi}{2}\right)}{1 + 2x^\alpha \cos\dfrac{\alpha\pi}{2} + x^{2\alpha}} & (2\,a) \\ \varepsilon'' = \Delta\varepsilon \dfrac{x^\alpha \sin\dfrac{\alpha\pi}{2}}{1 + 2x^\alpha \cos\dfrac{\alpha\pi}{2} + x^{2\alpha}} & (2\,b) \end{cases}$$

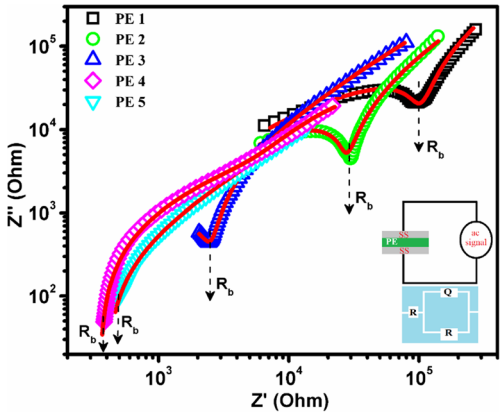

Fig. 4 Log-log plots of the complex impedance (Z'' vs. Z') for the pure PEO (PE 1), polymer salt complex (PE 2), and x wt.% SN ($x = 10, 15, 20$); (PE3, PE 4, PE 5)

Here, ε_s is static dielectric constant ($x \to 0$), ε_∞ is dynamic dielectric constant ($x \to \infty$), $x = \omega\tau$; ω is angular frequency of applied field and τ is average Debye relaxation time. Here, α is distribution exponent of the material sample. All these parameters are evaluated by fitting the experimental data with these equations and are summarized in Table 4.

The variation of the dielectric constant (ε') against frequency for different solid polymer electrolyte is shown in Fig. 8a and solid red line is fit to experimental data. All the SPE shows good agreement between the experimental and fitted curve.

In Fig. 8 a, it may be noticed that at low-frequency rapid increase in ε' is observed attributed to the accumulation of the charge at the electrode/electrolyte interface due to the

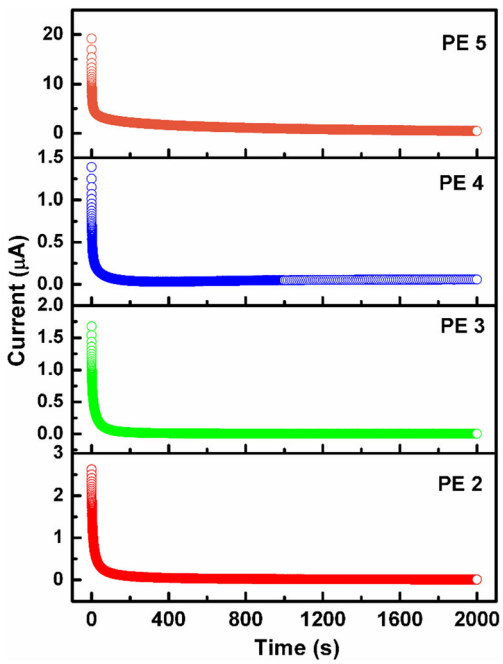

Fig. 5 Ion transference number plots for the prepared solid polymer electrolytes at room temperature

availability of sufficient time for orientation on the application of the field [60]. While at the high frequency, a decrease in dielectric constant is observed with the increase of frequency. This may be due to the blockage of ion diffusion or migration because of fast periodic reversal of the electric field. Now, the dipoles are unable to orient themselves in the applied field direction. This eliminates the electrode polarization and dominance of relaxation mechanism occurs, which leads to a steady state at high frequency [27, 61–64]. The absence of peak confirms the increase in conductivity which is due to enhanced ion mobility [65–67].

In the case of solid polymer electrolytes, two sources of dipoles exist, (i) salt dissociation produce cation-anion and (ii) polar groups of the polymer chain. The increased charge accumulation on the blocking electrodes in the low-frequency window is mainly due to cation/anion migration (first source) toward electrodes on the application of the field. The second source of dipoles in the polar group of the polymer chain makes conformational changes [68]. So, both phenomena together result in the enhancement in the dielectric constant of about $\sim 10^4$, and comparatively higher dielectric constant is observed for SN-based SPE ($\sim 30 \times 10^4$) as compared to polymer salts system ($\sim 4 \times 10^4$). Now, after the addition of salt in the pure PEO, dielectric constant increases due to the enhancement of the amorphous content. Further addition of SN in the polymer salt matrix increases the dielectric constant. This is evidenced from Table 4, which shows increase dielectric strength ($\Delta\varepsilon = \varepsilon_s - \varepsilon_\infty$) after SN addition (Fig. 8b). This may be due to three reasons, (i) disruption of the crystalline arrangement of host polymer chains, (ii) enhancement of amorphous content, and (iii) decrease of viscosity of polymer chain due to disruption of covalent bonding between polymer chains after SN penetration. Figure 9 shows the dependence of dielectric strength and dc conductivity on the concentration. The increase of the dielectric strength reflects the increase in the number of the charge carriers that increases the ion polarization. Also, the solid polymer electrolyte having the highest ionic conductivity possesses highest dielectric strength. This suggests that the increase in the ionic conductivity is due to increase in number of charge carriers and is associated with dielectric constant [69, 70]. In polymer electrolytes, the number of charge carriers depends on the dissociation energy and the dielectric constant by equation $n = n_o \exp\left(-\frac{U}{\varepsilon' kT}\right)$ [14–20, 71]. Here, k is Boltzman constant, T is absolute temperature and n_o is pre-exponential constant. This confirms the direct relation of the free ions and dielectric constant. The enhancement of the dielectric constant also evidences the presence of high amorphous content and increase in polarization. High dielectric constant value also promotes the ion dissociation which lowers ion aggregation tendency [72].

Table 3 Different contributions of electrical, electronic, ionic conductivity, transference number, and voltage stability window of SPE

Sample code	Transference number	Electrical conductivity (S cm^{-1})	Electronic conductivity (S cm^{-1})	Ionic conductivity (S cm^{-1})	Voltage stability window (V)
PE 1	–	4.95×10^{-8}	–	–	–
PE 2	0.98	1.95×10^{-7}	3.90×10^{-9}	1.91×10^{-7}	3.37
PE 3	0.97	2.80×10^{-6}	8.40×10^{-8}	2.71×10^{-6}	3.92
PE 4	0.98	1.92×10^{-5}	3.84×10^{-7}	1.88×10^{-5}	3.79
PE 5	0.99	1.44×10^{-5}	1.44×10^{-7}	1.42×10^{-5}	3.40

This evidences the perfect correlation between the dielectric constant and amorphous content, and hence the ionic conductivity. It suggests that the dielectric constant plays an effective role in the enhancement of the dc conductivity, and dielectric spectroscopy is an important technique to explain conductivity behavior [73, 74].

Another important parameter is the relaxation time. The low value of relaxation time results in the faster ion migration via chain segmental motion. The relaxation time ($\tau_{\varepsilon'}$) was extracted from the fitting of experimental data, and the optimized sample shows the lowest value of relaxation time [73, 75–77]. Another relaxation time, i.e., molecular relaxation time (τ_M) was obtained using the equation, $\tau_M = [(2\varepsilon_s + \varepsilon_\infty)/3\varepsilon_s] \times \tau_{\varepsilon'}$. It is interesting to note that, the molecular relaxation time is also lowest for the optimized system and is in proper agreement with the relaxation time ($\tau_{\varepsilon'}$), dielectric strength ($\Delta\ \varepsilon$), and ionic conductivity. It is observed from the previous results that the highest dc conductivity, dielectric constant, and lowest relaxation time are obtained for the 15% SN, which is in perfect agreement with the XTD and FTIR results.

The frequency dependent imaginary part of the dielectric permittivity or dielectric loss (ε'') is shown in Fig. 8c. The high value of the dielectric loss is due to the dc conductivity (free ion migration) that is associated with the electrode/electrolyte interface region. It is observed that the dielectric loss (ε'') value decreases with the increase of frequency for all solid polymer electrolytes owing to the absence of ion diffusion in field direction [78]. This also results in conductivity dispersion at high frequency owing to the absence of the electric polarization. The experimental data are in good agreement to the fitted data shown by a red solid line. As at high frequency, periodic reversal of field occurs that generates internal heat due to friction. Besides this, the dipoles are insufficient to orient

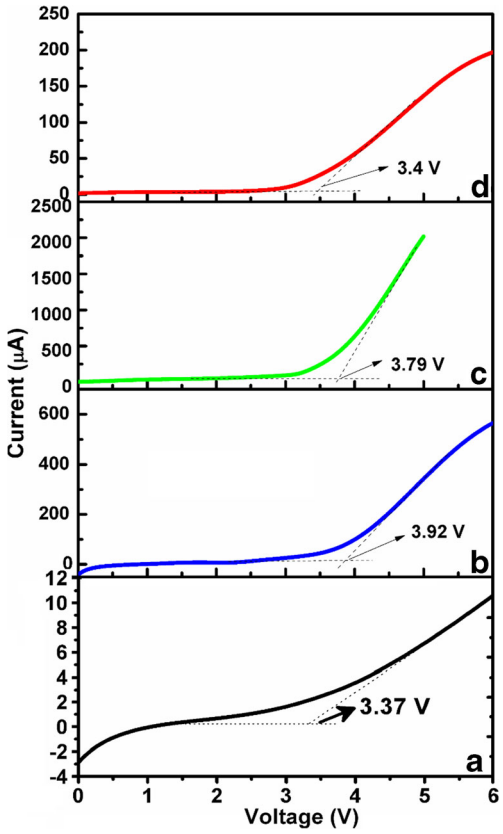

Fig. 6 Linear sweep voltammetry for the **a** PE 2, **b** PE 3, **c** PE 4, and **d** PE 5 in the configuration SS||SPE||SS

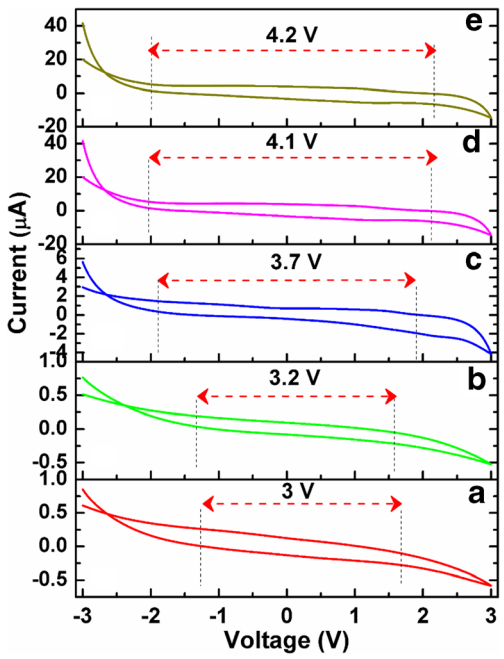

Fig. 7 Cyclic voltammetry of the **a** PE 1, **b** PE 2, **c** PE 3, **d** PE 4, and **e** PE 5 in the configuration SS/SPE/SS

Table 4 Various parameters obtained from fitting of ε' (ε_∞, $\Delta\varepsilon$, $\tau\varepsilon$, α) and ε'' ($\Delta\varepsilon$, $\tau\varepsilon''$,α) plot at room temperature

Sample code	ε'					ε''		
	ε_∞	$\Delta\varepsilon$ ($\times 10^3$)	$\tau_{\varepsilon'}$ (μs)	τ_M (μs)	α	$\Delta\varepsilon$ ($\times 10^3$)	$\tau_{\varepsilon''}$ (μs)	α
PE 1	20	10.27	1.69	1.12	0.83	19.93	1.82	0.78
PE 2	189	91.16	0.57	0.37	0.64	401.70	1.08	0.63
PE 3	1152	124.47	0.20	0.13	0.48	430.74	0.87	0.42
PE 4	1865	940.54	0.09	0.05	0.53	3998.57	0.26	0.52
PE 5	75	116.82	0.61	0.40	0.52	3356.01	0.52	0.56

along field direction and contribute to dielectric loss dielectric loss [79, 80]. This dielectric loss increases with an increase in a number of charge carriers as evidenced from Fig. 8b and becomes frequency independent at high frequency. The decrease in both dielectric constant (ε') and dielectric loss (ε'') reflects the non-Debye behavior shown by present solid polymer electrolyte system [81].

Sigma (σ'' vs. σ') representation

The sigma representation is crucial for getting an insight of the dispersion region at a high frequency in the Cole-Cole plot and is the plot of imaginary part (σ'') vs. real part (σ') conductivity [82]. The complex conductivity is expressed as $\sigma(\omega) = \sigma' + i\sigma''$,where, σ', σ'' are the real parts of conductivity, imaginary part of conductivity (Fig. 10a–e). As the complex electrical conductivity can be written using following expression (Eq. 3);

$$\begin{cases} \sigma(\omega) = \sigma' + i\sigma'' & (3\,a) \\ \sigma_\infty = \sigma_o + \frac{\varepsilon_v(\varepsilon_o - \varepsilon_\infty)}{\tau} = \sigma_o + \delta & (3\,b) \\ \sigma_{ac} = \sigma' = \omega\varepsilon_v\varepsilon'' \text{ and } \sigma_{dc} = \sigma'' = \omega\varepsilon_v\left(\varepsilon' - \varepsilon_\infty\right) = \omega\varepsilon_v\varepsilon' & (3\,c) \\ r = \frac{\delta}{2} = \frac{\varepsilon_v(\varepsilon_o - \varepsilon_\infty)}{2\tau} & (3\,d) \end{cases}$$

Here, σ' is the real part of conductivity, σ'' is the imaginary part of conductivity, ω is the angular frequency, r is the radius of the semicircle. And, when $\sigma'' = 0$ then low frequency x-intercept gives dc conductivity (σ_o) and high frequency x-intercept gives σ_∞. The radius of the semicircle (r) is inversely proportional to the relaxation time (τ). In the sigma representation, the radius of the semicircle (r) is inversely proportional to the relaxation time (τ). Table 5 summarizes the various parameters obtained from the plot. It is apparent from the Table 5 and Fig. 10 that the diameter of the semi-circle increases with addition of SN in the polymer salt complex. This implies the decrease of relaxation time ($r \propto 1/\tau$), as r value is

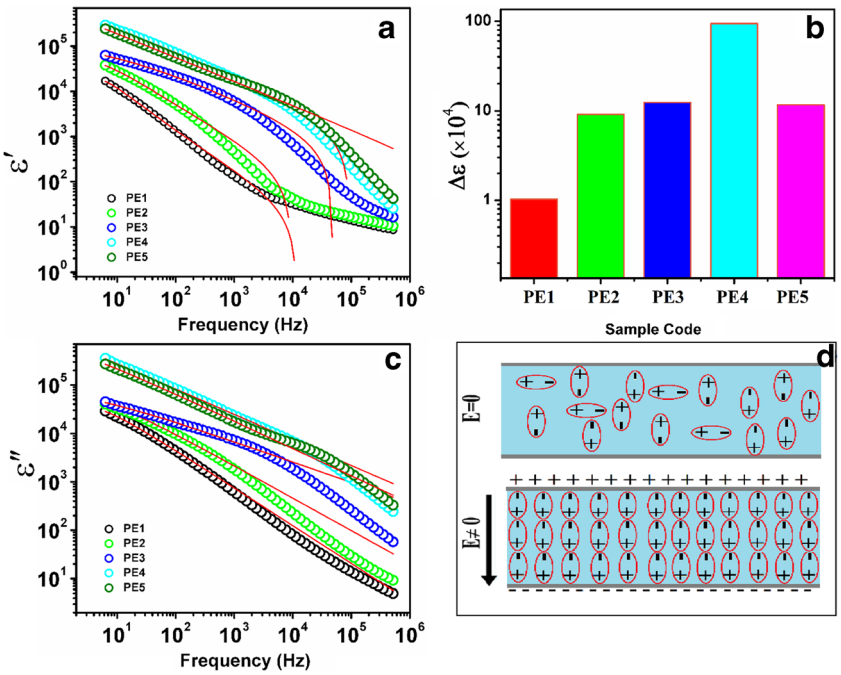

Fig. 8 Frequency dependence of the **a** dielectric constant ($\boldsymbol{\varepsilon}'$) for the polymer salt + x wt.% SN, **b** variation of $\Delta\varepsilon$ with for various SPE, **c** frequency dependence of the dielectric constant ($\boldsymbol{\varepsilon}''$), and **d** polarization mechanism. Solid lines are the best fit to the experimental data in **a** and **b**

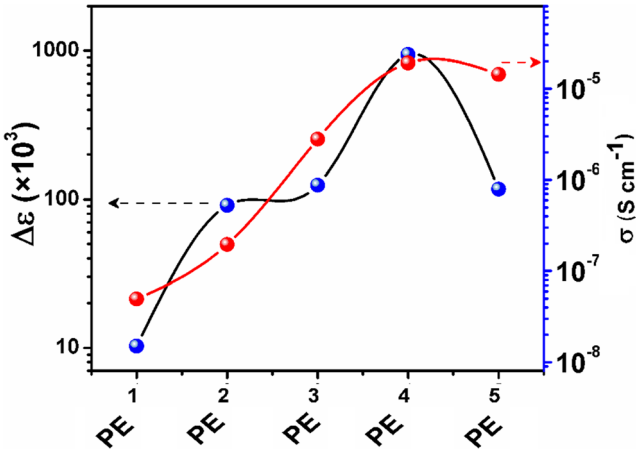

Fig. 9 Plot of dielectric strength and dc conductivity for different SPE system

highest for the PE 4 system which exhibits the highest ionic conductivity also. It suggests that Sigma representation provides sufficient evidence of the faster ion migration for PE 4 system, and decrease in relaxation time follows the trend of relaxation time ($\tau\,\varepsilon_r$) and molecular relaxation time (τ_M).

The real part of the complex conductivity

The complex conductivity of the solid polymer electrolytes is expressed as; $\sigma^*(\omega) = \sigma'(\omega) + i\sigma''(\omega)$, *where* real part is expressed as $\sigma' = \sigma_{ac} = \omega\varepsilon_o\varepsilon'' = \omega\varepsilon_o\varepsilon' \tan\delta$, and imaginary part as $\sigma'' = \omega\varepsilon_o\varepsilon' = \omega\varepsilon_o\varepsilon'' \tan\delta$. Here ω, ε_o, ε'' are the angular frequency, dielectric permittivity of the free space, and dielectric loss. In case of polymer electrolytes ion migration occurs

Table 5 The measured parameter, σ_o, σ_∞, δ, and r from the plot of σ'' vs. σ' for various SPEs at RT

Sample code	σ_o (S cm^{-1})	σ_∞(S cm^{-1})	δ ($\times10^{-7}$)	r ($\times10^{-7}$)
PE 1	6.12×10^{-9}	7.03×10^{-8}	0.64	0.32
PE 2	1.59×10^{-8}	2.01×10^{-7}	1.85	0.92
PE 3	1.27×10^{-7}	2.75×10^{-6}	26.23	13.11
PE 4	0.63×10^{-6}	1.62×10^{-5}	155.82	77.91
PE 5	0.13×10^{-6}	1.21×10^{-5}	119.71	59.85

through two phenomena, (i) ion migration via the coordinating sites provided by polymer chain and (ii) segmental motion of polymer chain [83, 84]. To obtain further information about the ion migration and dielectric parameters, the real part of the conductivity has been simulated with a model proposed by Roy et al. [85, 86]. One advantage with this model is that it provides information in the whole frequency window, as Jonscher power law is limited to high frequency only. According to this model, the effective complex conductivity can be written as

$$\sigma^*_{\text{eff}} = \left(\frac{1}{\sigma_b} + \frac{1}{i\omega C_{\text{dl}}}\right)^{-1} + i\omega C_b \tag{4}$$

Now, considering the Eq. 4, the real part of the conductivity can be written as

$$\sigma'(\omega) = \frac{\sigma_b^2 C_{\text{dl}}\omega^\alpha \cos\left(\frac{\alpha\pi}{2}\right) + \sigma_b (C_{\text{dl}}\omega^\alpha)^2}{\sigma_b^2 + 2\sigma_b C_{\text{dl}}\omega^\alpha \cos\left(\frac{\alpha\pi}{2}\right) + (C_{\text{dl}}\omega^\alpha)^2} \tag{5}$$

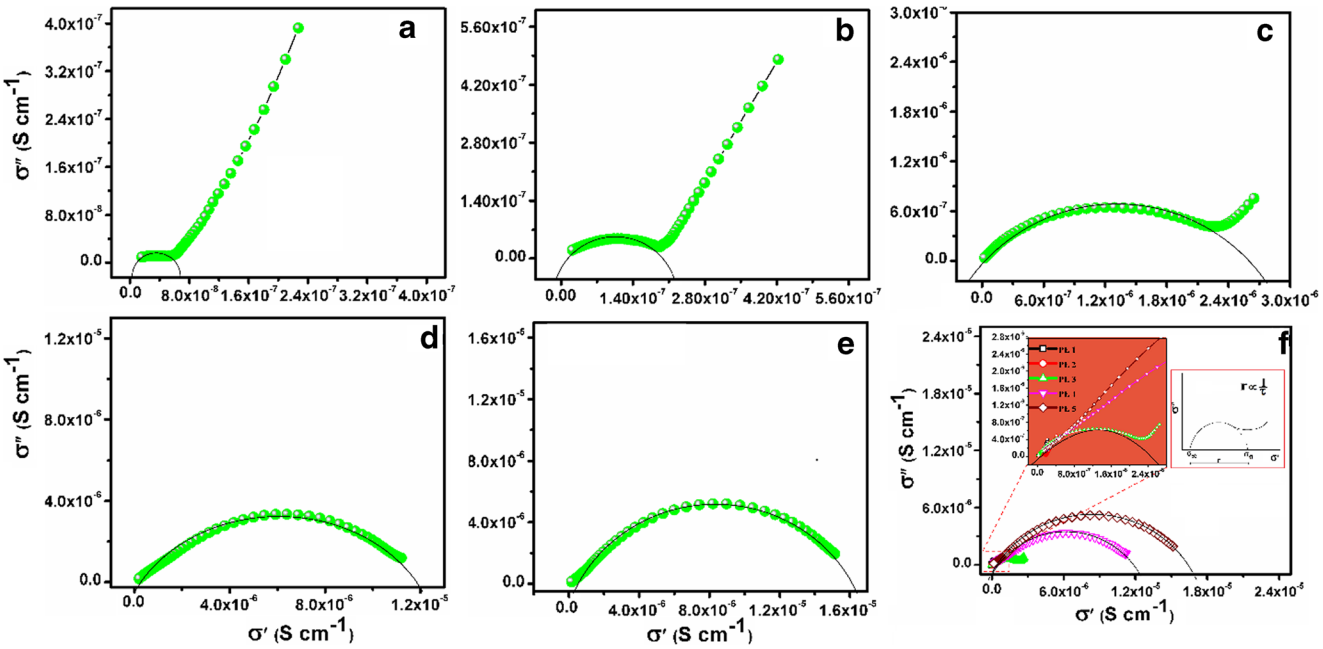

Fig. 10 Sigma representation (σ'' vs. σ') of the **a** PE 1, **b** PE 2, **c** PE 3, **d** PE 4, **e** PE 5, and **f** comparative plot of all solid polymer electrolyte

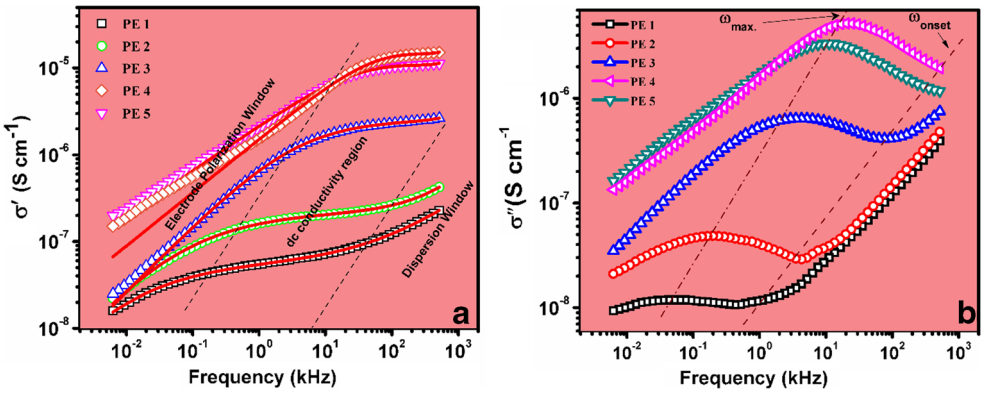

Fig. 11 Frequency-dependent **a** real part (σ'), and **b** imaginary part ((σ'') of complex conductivity for solid polymer electrolyte. Solid lines are absolute fit to experimental data points. The dotted line shows the change in ω_{max} and ω_{on} with SN content

The high-frequency Jonscher power law expression is also included in the real and imaginary part of conductivity

$$\sigma'(\omega) = \sigma_b\left[1 + \left(\frac{\omega}{\omega_h}\right)^n\right] \quad (6)$$

Here, both n and s have a value less than unity. For complete frequency window analysis, we replace the σ_b in Eq. 5 by Eq. 6, and this final equation is used for fitting the experimental results. Where, C_{dl} is frequency independent double layer capacitance, ω is the angular frequency, s and α are exponent terms with value < 1 and C_b is the bulk capacitance of solid polymer electrolyte.

The variations of real (σ') and imaginary part (σ'') of the complex conductivity as a function of frequency for PEO electrolyte with varying content of SN are shown in Fig. 11a and b. The plot infers the increase of ac conductivity with frequency and three distinct regions are identified, (i) low frequency electrode-polarization region, (ii) frequency independent plateau region in intermediate frequency, and (iii) high-frequency dispersive region. In the low frequency, ac conductivity increases with frequency and is the result of dominance of the electrode polarization phenomena due to sufficient time to dipoles for orientation. The intermediate frequency plateau region is associated with the dc conductivity and implies the long-range ion migration. This indicates that the impedance spectroscopy is powerful technique to understand the ion transport in polymer electrolytes [87]. Then, the high frequency dispersion region is observed corresponding to the ion migration by hopping mechanism, i.e., short-range ion migration. This switch from the intermediate region to dispersive region occurs at particular frequency, i.e., hopping frequency (ω_h). It may be noted that for pure PEO, all three regions appears, but after addition of SN, the high frequency dispersive region disappears. This implies that the ω_h shifts toward the higher frequency with addition of SN [88–91]. The high frequency dispersion region is associated with the short-range ion migration due to charge carrier's confinement in the potential wells. This is in correlation with the impedance plots which shows the disappearance of the high frequency arc (associated with bulk properties) with addition of SN in polymer salt complex. This suggests that the ac conductivity is a bulk property of material and provides evidence of the type of conduction mechanism in polymer electrolytes. It reflects that the ion migration in solid polymer electrolyte is the combined effect of the hopping process and segmental motion of polymer chains [92]. To obtain more crucial information, the complex conductivity plot is fitted by the equation proposed by Roy et al. [85] which also included the universal Jonscher power law which provides details only of the high frequency region. So, we have fitted the ac conductivity plot in the whole frequency window, shown by solid line in the plot [58, 85].

Figure 11 a shows the fitted plot of frequency dependent conductivity in the whole frequency window (shown by solid line) using σ_b, ω_h, α, and n as variable parameters. It may be noted that both the experimental and fitted plots are in good

Table 6 Comparison of fitted parameters for real part of the complex conductivity for different PEs at RT.

Sample code	Conductivity ($\times 10^{-6}$ S cm^{-1})		ω_h ($\times 10^5$)	α	n	C_{dl} (μF)	τ_h (μs)
	ac	Bulk					
PE 1	0.05	0.04	0.52	0.57	0.48	0.02	19.1
PE 2	0.22	0.19	3.71	0.85	0.47	0.03	2.69
PE 3	0.95	2.80	8.13	0.38	0.77	1.66	1.23
PE 4	1.42	19.2	15.17	0.26	0.79	21.1	0.65
PE 5	1.12	14.4	9.13	0.31	0.98	14.2	1.09

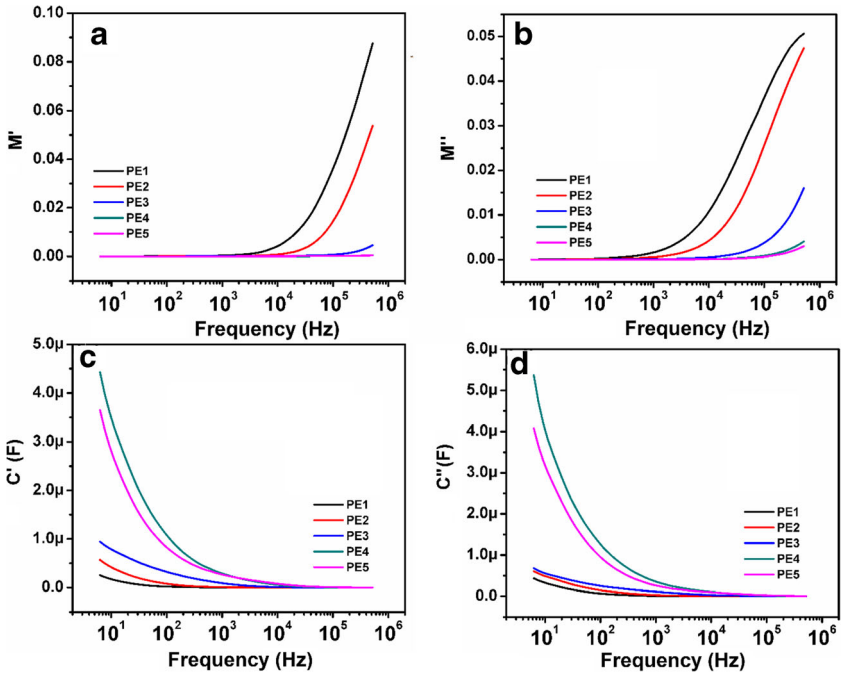

Fig. 12 Frequency-dependent **a** real part ($M^{'}$), (**b**) imaginary part of the modulus ($M^{''}$), **c** real part ($C^{'}$), and **d** imaginary part of capacitance ($C^{''}$) for various PEs at room temperature

agreement with each other. The fitted parameters (σ_b, ω_h, α, n) are summarized in Table 6 at room temperature. It may observed from Table 6 that, hopping frequency (ω_h) increases when salt is added in the pure PEO and increases further addition of SN. The high hopping frequency for the PE4 suggests the higher dc conductivity due to lowering of hopping relaxation time (τ_h) for this system and is in agreement with the impedance study [85]. The increase in the conductivity is also related to increase in the disorder in the polymer chain arrangement after SN addition. For further strengthening the result, a correlation of various fitted parameters has been built in the upcoming section with the ionic conductivity. This suggests that addition of SN increases the polymer flexibility and hopping of cation from one coordinating site is faster. For, $\omega > \omega_h$, the two processes may occur, (i) correlated forward-backward-forward hopping (unsuccessful hopping) and (ii) ion migration to the new coordinating site (successful hopping) [93–95]. The correlated forward-backward-forward hopping reflects the insufficient time to the cation to move to next coordinating site and results in dispersion in the high frequency window. It is also noted that value of both exponent parameters is less than unity. Decrease in the value of α indicates the ion migration via hopping process and is explained by correlated barrier hopping (CBH) model [96].

The frequency dependent imaginary part (σ'') of the complex conductivity is shown in Fig. 11b. The plot is divided in the region depending on two frequencies, onset frequency (ω_{on}) and maximum frequency (ω_{max}), (i) low frequency electrode polarization (EP) region, (ii) intermediate frequency dc conductivity region, and (iii) high-frequency dispersion region. It may be observed from the plot that as we move from right to left on frequency axis, the decrease in the $\sigma^{''}$ occurs and a minima $\sigma^{''}$ is associated with the onset frequency (ω_{on}) linked with onset of electrode polarization. At this frequency, electrode polarization starts to build up and on moving toward decreasing frequency, maxima in $\sigma^{''}$ is observed associated with the maximum frequency (ω_{max}). It implies that, at this frequency, maximum polarization is achieved [95, 97–100]. It is also observed $\sigma^{'}$ starts decreasing when the maxima in $\sigma^{''}$ is observed as evidenced from Fig. 11a and b. Also, the polarization region in Fig. 11b is wider for SN-doped polymer salt matrix as compared to the SN free, i.e., polymer salts matrix. It may be concluded that the addition of SN plays effective role in enhancing the dielectric properties and cation migration in the solid polymer electrolyte.

Modulus study

The suppressed electrode polarization region in the complex permittivity is analyzed by using the modulus formalism in the whole frequency window. The modulus data is expressed in terms of reciprocal of complex permittivity and is expressed as $M^* = 1/\varepsilon^* = M^{'} + jM^{''}$.

Real and imaginary part of Modulus

Figure 12a and b show the variation of the real ($M^{'}$) and imaginary ($M^{''}$) parts of complex modulus against the frequency. In case of polymer electrolytes, the ion migration via coordinating sites alters the electric potential of the surrounding environment, which further influences the other ions. This process results in the spread of the relaxation peak

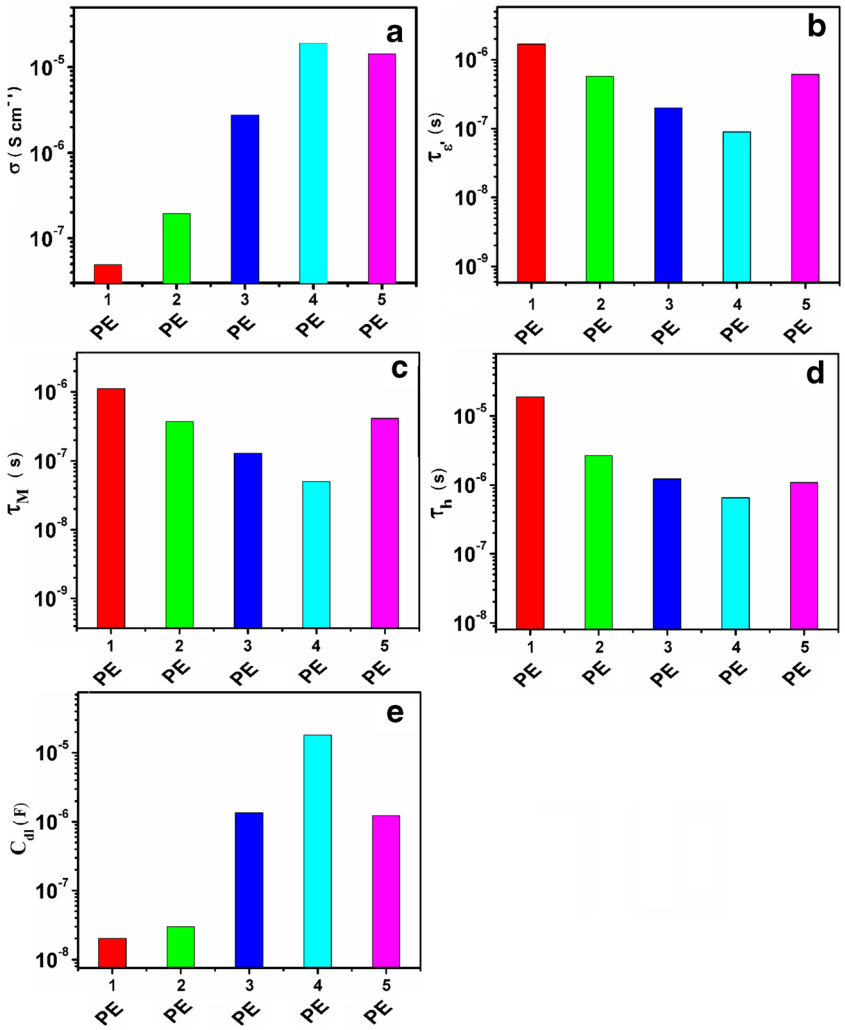

Fig. 13 Correlation of **a** ionic conductivity (σ), **b** $\tau_{\varepsilon'}$, **c** τ_M, **d** τ_h, and **e** double-layer capacitance (C_{dl})

[101]. A long tail is observed in the low frequency window corresponding to $M' \rightarrow 0$, and increase in the length of tail evidenced the large value of electrodes polarization capacitance [101, 102]. A similar result has been reported by Arof et al. [103]. At high-frequency sharp increase in Fig. 12a and b indicates the dispersion region (presence of relaxation time) owing to the low probability of ion responding to applied field [31, 104, 105]. Although there is small peak in the pure polymer and disappears with addition of salt and SN, this peak is corresponding to the transition from the long-range migration (translation) to short-range ion migration (dipolar) and lies beyond the measured range which evidences the non-Debye type nature. There is no peak in the dielectric loss spectra that evidences the coupled ionic and segmental motion [106–108]. The rapid increase in Fig. 12b at high frequency is attributed to the ion hopping from one coordinating site to another. The lower value in modulus spectra (M'') as in Fig. 12 b is an indication of fast ion migration and is evidenced by the modulus relaxation time (τ_m) that shows minima for the PE4 system. The lowering of the relaxation time reflects the highest ionic conductivity for this system [109]. Further, the real (C') and imaginary (C'') part of the capacitance are obtained using the equation; $C'(\omega) = Z''/\omega(|Z(\omega)|)^2$, $C''(\omega) = Z'/\omega(|Z(\omega)|)^2$; here, Z' and Z'' are the real and imaginary parts of impedance and ω is angular frequency ($=2\pi f$). Real part of capacitance indicates the storage of ions while imaginary part is associated with the energy loss in the polymer electrolyte [110]. The variation of the real and imaginary part of capacitance is shown in Fig. 12c and d. For, all the solid polymer electrolytes, the real and imaginary part of capacitance decreases with frequency. Figure 12 c and d depicts the plot of real and imaginary part of capacitance against the frequency. It is observed that both component show decreasing trend with an increase of the frequency. The addition of SN in the polymer salt matrix increases the ions in the polymer matrix that contributed to capacitance, and highest capacitance is observed for the PE4 system. The highest capacitance is associated with the polymer electrolyte with highest ionic conductivity and is in perfect correlation with the dielectric constant value.

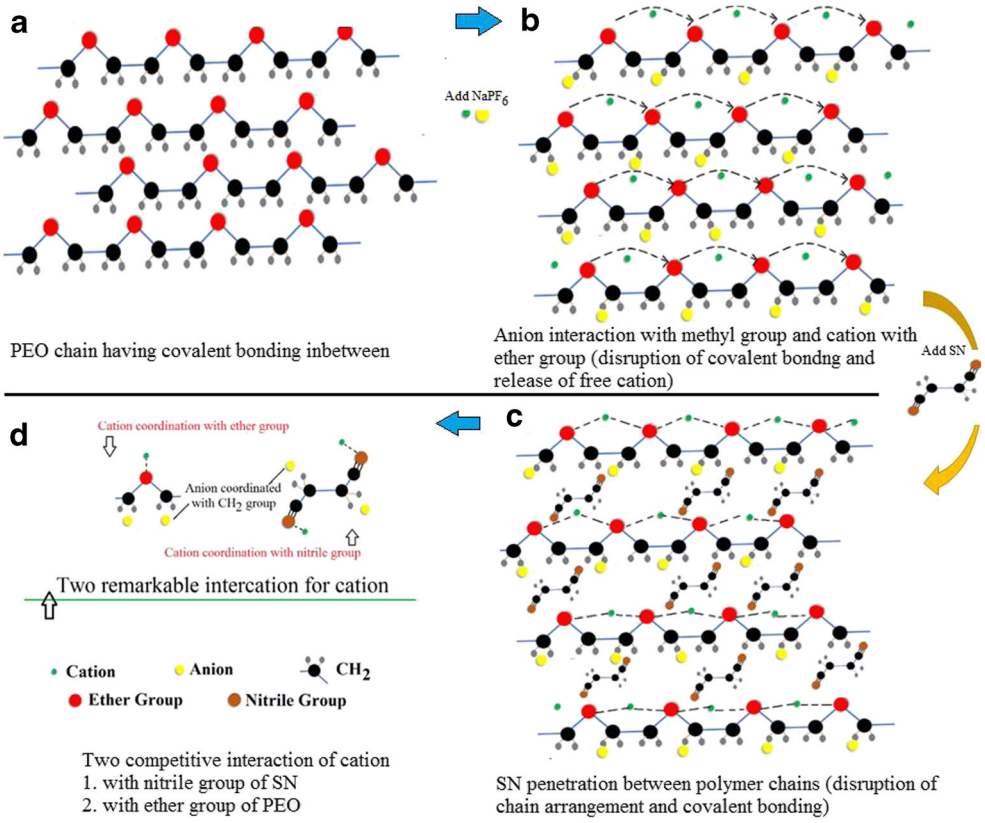

Fig. 14 Proposed scheme for the cation transport. **a** Pure PEO polymer chain. **b** Cation coordination with PEO. **c** Interaction between nitrile group of SN, PEO, and cation. **d** Two competitive interactions of cation

Correlation of ionic conductivity (σ) with double layer capacitance (C_{dl}), and various relaxation times ($\tau_{\varepsilon'}$, τ_M, τ_h)

It was concluded from the above discussion that the ionic conductivity is linked with the relaxation time and number of charge carriers. So, correlation of the ionic conductivity is built-up with relaxation time ($\tau_{\varepsilon'}$, τ_M, τ_h) obtained by a different process (Fig. 13). Figure 13a, shows the variation of ionic conductivity with SN content and shows maxima for 10 wt.% SN content. This maximum may be due to the increase in the number of ions participating in the conduction. It reflects the crucial role played by the SN on altering the polymer matrix and the polymer flexible that promotes the faster ion migration from one coordinating site to another. While at high SN content decrease in the conductivity is due to the dominance of the plastic nature which shows a negative effect. At optimized content-enhanced polymer flexibility promotes the faster ion migration from one coordinating site to another.

While at high SN content decrease in the conductivity is due to the dominance of the plastic nature which shows a negative effect. Figure 13b and d show the variation of the relaxation time (dielectric relaxation time, molecular relaxation time, hopping time) against the SN content. It may be noted that the optimized system (PE4) shows minima in all relaxation time. The lowering of the relaxation time implies that at this content, maximum number of ions are available for migration, as well as faster chain segmental motion is observed due to reduced viscosity of polymer chains. The variation of the double layer capacitance with SN content is shown in Fig. 13e and is maximum for the PE4 system. As capacitance is related to the storage capacity of ions, so it suggests that the present system has a large number of free ions. In conclusion, it may be stated that the lowering of the relaxation time and maxima in the ionic conductivity is a result of the presence of the polar nitrile group in the SN. All results are in absolute correlation with each other.

Ion transport mechanism

To understand the role of the SN in improving the properties of the polymer matrix, an ion transport scheme is proposed. The constituents of the solid polymer electrolyte are PEO, NaPF6, and SN. Figure 14 a shows the pure PEO chains and are crystalline in nature. Now, when salt is added in the pure PEO, then the salt get dissociated in the cation (red circle) and anion (yellow circle). Two possible interactions exists here, (i) As cation (Na^+) is Lewis acid, it has tendency to coordinate to the ether group of the polymer chain, and (ii) as anion (PF_6^-) is bulky in size, it remains in immobilized state and attached with the polymer backbone (Fig. 14b). This makes polymer salt complexation as evidenced by the FTIR analysis. Now, when SN is

added to the polymer salt matrix. Now, when the addition of SN is done in polymer salt matrix, then the presence of highly polar nitrile group (C ≡ N) in the SN alters the significant interaction between the polymer and salt. Two possibilities are (i) cation coordination with ether group of PEO and (ii) cation coordination with nitrile group. But, cation has more tendency to interact with ether group than nitrile due to high electronegativity of oxygen as compared to nitrogen. As another key effect of SN is that it may penetrate in between the polymer chains and disrupt the covalent bonding between them. It results in the enhanced free volume for the ion migration and promotes the faster ion migration (Fig. 14c, d) by reducing the viscosity of polymer chains. Same has been evidenced by the XRD analysis.

Conclusions

The effect of SN on the structural, electric, and dielectric properties in PEO-$NaPF_6$ + SN-based solid polymer electrolyte prepared by solution cast technique has been investigated. The morphological, structural, electrochemical, and dielectric properties were investigated in detail. The XRD analysis suggests the enhancement of the amorphous content on the addition of SN and is supported by the FESEM analysis. The complex formation was confirmed by the FTIR and interactions between the polymer; salt is influenced by the SN addition. The highest ionic conductivity has been found to be 2×10^{-5} S cm^{-1} (@RT) for the 10 wt.% SN-doped (PE4) solid polymer electrolyte. The ion transference number was close to unity for all systems (0.99), and voltage stability window was about 4 V which is within the desirable limit for the solid-state battery applications. The polymer electrolyte system with the highest ionic conductivity (PE4) has the highest dielectric constant and infers the high storage capacity. The lowering of the relaxation time evidences the faster segmental motion of the polymer chain. The real part of ac conductivity has been analyzed in the whole frequency window including the low-frequency electrode polarization region and high-frequency dispersion region. The optimized system having high conductivity shows the lowest relaxation time ($\tau_{\varepsilon'}$, τ_M, τ_h) and is in good agreement with double-layer capacitance and high dielectric constant value. The modulus spectra evidence the presence of single relaxation and increased capacitance. The ionic conductivity shows one-to-one correspondence with the relaxation time and double-layer capacitance and confirms the PE4 as an optimized system. Finally, an ion transport scheme has been proposed to highlight the role of SN in modifying the interactions between polymer and salt.

Acknowledgments One of the authors (AA) thankfully acknowledges the Central University of Punjab, Bathinda for providing the fellowship.

References

1. Ellis BL, Nazar LF (2012) Curr Opin Solid State Mater Sci 16: 168–177
2. Che H, Chen S, Xie Y, Wang H, Amine K, Liao XZ, Ma ZF (2017) Energy Environ Sci 10:1075–1101
3. Koduru HK, Marino L, Scarpelli F, Petrov AG, Marinov YG, Hadjichristov GB et al (2017) Curr Appl Phys 17:1518
4. Q. Bai, L. Yang, H. Chen, Y. Mo,(2018) Advanced energy materials 1702998
5. Arya A, Sharma AL (2019) J Solid State Electrochem. https://doi.org/10.1007/s10008-019-04203-x
6. Pradhan DK, Samantaray BK, Choudhary RNP, Thakur AK (2005) Ionics 11:95–102
7. Pitawala HMJC, Dissanayake MAKL, Seneviratne VA, Mellander BE, Albinson I (2008) J Solid State Electrochem 12:783–789
8. Arya A, Sadiq M, Sharma AL (2018) Ionics 24:2295–2319
9. Sharma AL, Thakur AK (2013) Ionics 19:795–809
10. Arya A, Sharma AL (2017) Ionics 23:497–540
11. Chaurasia SK, Kataria S, Gupta AK, Verma YL, Singh VK, Tripathi AK, Saroj AL, Singh RK (2014) RSC Adv 5:8263
12. Dhatarwal P, Sengwa RJ, Choudhary S (2019) SN Appl Sci 1:112
13. Tan SM, Johan MR (2011) Ionics 17:485–490
14. Wan J, Xie J, Mackanic DG, Burke W, Bao Z, Cui Y (2018) Mater Today Nano 4:1–16
15. Sharma AL, Thakur AK (2011) J Mater Sci 46:1916–1931
16. Pritam A, Arya A, Sharma L (2019) J Mater Sci 54:7131–7155
17. Bresser D, Passerini S, Scrosati B (2013) Chem Commun 49: 10545–10562
18. Arya A, Sharma AL (2017) J Phys D Appl Phys 50:443002
19. Xue Y, Li X, Quesnel DJ (2017) Int J Electrochem Sci 12:10674
20. Laheäär A, Jänes A, Lust E (2012) Electrochim Acta 82:309–313
21. Arya A, Sharma AL (2018) J Solid State Electrochem 22:2725–2745
22. Alarco PJ, Abu-Lebdeh Y, Abouimrane A, Armand M (2004) Nat Mater 3:476–481
23. Aravindan V, Lakshmi C, Vickraman P (2009) Curr Appl Phys 9: 1106–1111
24. Karuppasamy K, Kim D, Kang YH, Prasanna K, Rhee HW (2017) J Ind Eng Chem 52:224–234
25. Hashmi SA, Upadhyaya HM, Thakur AK, Verma AL (2000) Ionics 6:248–259
26. Das A, Thakur AK, Kumar K (2013) Ionics 19:1811–1823
27. Choudhary S, Sengwa RJ (2013) Mater Chem Phys 142:172–181
28. Hashmi SA, Chandra S (1995) Mater Sci Eng B 34:18–26
29. Zhang C, Gamble S, Ainsworth D, Slawin AM, Andreev YG, Bruce PG (2009) Nat Mater 8:580–584
30. Kesavan K, Mathew CM, Rajendran S, Ulaganathan M (2014) Mater Sci Eng B 184:26–33
31. Mohamed Ali T, Padmanathan N, Selladurai S (2013) Ionics 19: 1115–1123
32. Subba Reddy CV, Sharma AK, Narasimha Rao VVR (2003) J Power Sources 114:338–345
33. Jinisha B, Anilkumar KM, Manoj M, Pradeep VS, Jayalekshmi S (2017) Electrochim Acta 235:210
34. Anantha PS, Hariharan K (2005) Solid State Ionics 176:155–162
35. Jonscher AK (1983) Dielectric relaxation in solids. Chelsea Dielectric, London
36. Tang R, Jiang C, Qian W, Jian J, Zhang X, Wang H, Yang H (2015) Sci Rep 5:13645

37. Arya A, Sharma AL, Sharma S, Sadiq M (2016) J Integrated Sci Technol 4:17
38. Sharma AL, Thakur AK (2010) J Appl Polym Sci 118:2743–2753
39. Kim S, Hwang EJ, Park SJ (2008) Curr Appl Phys 8:7209
40. Rai A, Sharma AL, Thakur AK (2014) Solid State Ionics 262: 230–233
41. Jacob MME, Prabaharan SRS, Radhakrishna S (1997) Solid State Ionics 104:267–276
42. Hema M, Tamilselvi P (2016) J Phys Chem Solids 96:42
43. Verma ML, Minakshi M, Singh NK (2014) N, Electrochimica Acta 137:497
44. Barmi MJ, Minakshi M (2016) Chem PlusChem 81:964–977
45. Marzantowicz M, Dygas JR, Krok F, Łasińska A, Florjańczyk Z, Zygadło-Monikowska E, Affek A (2005) Electrochim Acta 50: 3969
46. Aziz SB, Faraj MG, Abdullah OG (2018) Sci Rep 8:14308
47. Sharma AL, Shukla N, Thakur AK (2008) J Polym Sci Part B Polym Phys 46:2577
48. Wagner JB, Wagner CJ (1957) Chem Rev 20:1597
49. Evans J, Vincent CA, Bruce PG (1987) Polymer 28:2324–2328
50. Bhargav PB, Mohan VM, Sharma AK, Rao VVRN (2009) Curr Appl Phys 9:165–171
51. Arya A, Sharma AL (2018) J Phys D Appl Phys 51:045504
52. Faridi M, Naji L, Kazemifard S, Pourali N (2018) Chem Pap 72: 2289–2300
53. Shalu SV, Singh RK (2015) J Mater Chem C 3:7305–7318
54. Balo L, Gupta H, Singh VK, Singh RK (2017) Electrochim Acta 230:123–131
55. Yang CC (2002) J Power Sources 109:22–31
56. Schrodle S, Annat G, MacFarlane DR, Forsyth M, Buchner R, Hefter G (2007) Aust J Chem 60:6
57. Izgorodina EI, Forsyth M, MacFarlane DR (2009) Phys Chem Chem Phys 11:2452
58. Arya A, Sharma AL (2018) J Phys Condens Matter 30:165402
59. Cole KS, Cole RH (1941) J Chem Phys 9:341–351
60. Sharma AL, Thakur AK (2009) Ionics 16:339
61. Truong VT, Codd AR, Forsyth M (1994) J Mater Sci 29:4331–4338
62. Sharma AL, Thakur AK (2015) Ionics 21:1561–1575
63. Sengwa RJ, Kaur K, Chaudhary R (2000) Polym Int 49:599–608
64. Abdelrazek EM, Elashmawi IS, Hezma AM, Rajeh A, Kamal M (2016) Phys B Condens Matter 502:48–55
65. Aziz SB (2018) J Inorg Organomet Polym Mater 28:1942–1952
66. Salleh NS, Aziz SB, Aspanut Z, Kadir MFZ (2016) Ionics 22: 2157–2167
67. Arya A, Sadiq M, Sharma AL (2018) Polym Bull. https://doi.org/10.1007/s00289-018-2645-y
68. Ravi M, Song S, Gu K, Tang J, Zhang Z (2015) Mater Sci Eng B 195:74–83
69. Gohel K, Kanchan DK (2018) Journal of Advanced Dielectrics 8: 1850005
70. Arya A, Sharma AL (2018) Macromol Res. https://doi.org/10.1247/s00125-018-26142
71. Woo HJ, Majid SR, Arof AK (2011) Solid State Ionics 199:14
72. K. C. Kao, (2004) Dielectric phenomena in solids. Elsevier
73. Aziz SB (2013) Iran Polym J 22:877–883
74. Aziz SB, Abidin ZHZ (2013) Journal of Soft Matter 323868
75. Choudhary S, Dhatarwal P, Sengwa RJ (2017) Indian J Eng Mater Sci 24:123
76. Ravi M, Pavani Y, Kiran Kumar K, Bhavani S, Sharma AK, Narasimha Rao VVR (2011) Mater Chem Phys 130:442–448
77. Salman F, Khalil R, Hazaa H (2014) Adv J Phys Sc 3:1
78. Morsi MA, El-Khodary SA, Rajeh A (2018) Phys B Condens Matter 539:88–96
79. Prasanna CS, Suthanthiraraj SA (2017) Ionics 23:3137–3150
80. R. J. Singh,(2012) Solid State Physics, Dorling Kindersley (India)
81. Shukur MF, Ibrahim FM, Majid NA, Ithnin R, Kadir MFZ (2013) Phys Scr 88:025601
82. Weia YZ, Sridhar S (1993) J Chem Phys 99:3119–3124
83. Di Noto V, Vittadello M (2002) Solid State Ionics 147:309–316
84. Aziz SB, Abidin ZHZ (2014) Mater Chem Phys 144:280–286
85. Roy A, Dutta B, Bhattacharya S (2016) RSC Adv 6:65434–65442
86. Arya A, Saykar NG, Sharma AL J Appl Polym Sci 136(2018): 47361
87. Aziz SB, Abdullah RM, Rasheed MA, Ahmed HM (2017) Polymers 9:338
88. Sharma AL, Thakur AK (2010) Ionics 17:135
89. Nasri S, Hafsia AB, Tabellout M, Megdiche M (2016) RSC Adv 6:76659–76665
90. Jonscher AK (1978) J Mater Sci 13:553–562
91. Papathanassiou AN, Sakellis I, Grammatikakis J (2007) Appl Phys Lett 91:122911
92. Aziz SB, Abidin ZHZ (2015) J Appl Polym Sci 132:41774
93. Pradhan DK, Choudhary RNP, Samantaray BK (2008) Int J Electrochem Sci 3:597
94. Shukla N, Thakur AK, Shukla A, Marx DT (2014) Int J Electrochem Sci 9:7644
95. Arya A, Sharma S, Sharma AL, Kumar D, Sadiq M (2016) Asian J Eng and App Tech 5(4)
96. Yang J, Meng XJ, Shen MR, Fang L, Wang JL, Lin T et al (2008) J Appl Phys 104:104113
97. Fuentes A, Andrio F, Teixidor C, Vinas V, Compan V (2017) Phys Chem Chem Phys 19:15177–15186
98. Khamzin AA, Popov II, Nigmatullin RR (2014) Phys Rev E Stat Nonlinear Soft Matter Phys 89:032303
99. Fragiadakis D, Dou S, Colby RH, Runt J (2008) Macromolecules 41:5723–5728
100. Baskaran R, Selvasekarapandian S, Hirankumar G (2004) Ionics 10:129–134
101. Arya A, Sharma AL (2018) J Mater Sci Mater Electron 29:17903
102. Agrawal SL, Singh M, Asthana N, Dwivedi MM, Pandey K (2011) Int J Polym Mater 60:276–289
103. Woo HJ, Majid SR, Arof AK (2012) Mater Chem Phys 134:755–761
104. Karmakar A, Ghosh A (2012) Curr Appl Phys 12:539–543
105. Dhatarwal P, Sengwa RJ (2017) J Polym Res 24:135
106. Aziz SB, Abdullah RM (2018) Electrochim Acta 285:30–46
107. Aziz SB (2015) Bull Mater Sci 38:1597–1602
108. Aziz SB (2016) Adv Mater Sci Eng 2527013. https://doi.org/10.1155/2016/2527013
109. Macedo PB, Moynihan CT, Bose R (1972) Phys Chem Glasses 13:171
110. Yadav M, Kumar M, Tiwari T, Srivastava N (2016) Ionics 23:2871